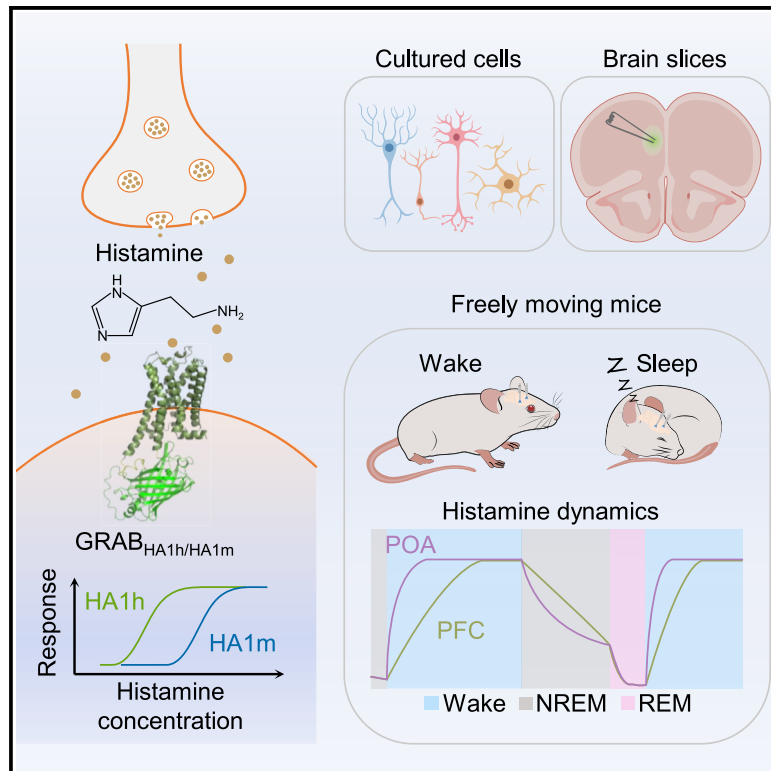# Neuron

Genetically encoded sensors for measuring histamine release both *in vitro* and *in vivo*

Graphical abstract

Authors

Hui Dong, Mengyao Li, Yuqi Yan, ..., Huan Wang, Rob Leurs, Yulong Li

Correspondence
yulongli@pku.edu.cn

In brief

Dong et al. develop and validate a pair of genetically encoded GPCR-activation-based histamine sensors, which enable monitoring of extracellular histamine dynamics in acute brain slices and freely behaving mice with high spatiotemporal resolution. Using these sensors, they find distinct patterns of histamine dynamics in two brain regions during sleep-wake cycles.

Highlights

- GRAB$_{HA}$ sensors are genetically encoded GPCR-activation-based histamine (HA) sensors

- GRAB$_{HA}$ sensors enable specific HA detection with high spatiotemporal resolution

- Two separate constructs expand the effective dynamic range of HA detection

- GRAB$_{HA}$ reveals distinct patterns of HA dynamics between different brain regions

CellPress

Neuron

NeuroResource

Genetically encoded sensors for measuring histamine release both *in vitro* and *in vivo*

Hui Dong,[1,2,7] Mengyao Li,[1,2,7] Yuqi Yan,[1,2,3] Tongrui Qian,[1,2] Yunzhi Lin,[1,2] Xiaoyuan Ma,[4] Henry F. Vischer,[4] Can Liu,[1,2] Guochuan Li,[1,2] Huan Wang,[1,2] Rob Leurs,[4] and Yulong Li[1,2,3,5,6,8,*]

[1]State Key Laboratory of Membrane Biology, Peking University School of Life Sciences, Beijing 100871, China
[2]PKU-IDG/McGovern Institute for Brain Research, Beijing 100871, China
[3]Peking-Tsinghua Center for Life Sciences, Academy for Advanced Interdisciplinary Studies, Peking University, Beijing 100871, China
[4]Division of Medicinal Chemistry, Faculty of Science, Amsterdam Institute of Molecular and Life Sciences, Vrije Universiteit Amsterdam, 1081 HZ Amsterdam, The Netherlands
[5]Chinese Institute for Brain Research, Beijing 102206, China
[6]National Biomedical Imaging Center, Peking University, Beijing 100871, China
[7]These authors contributed equally
[8]Lead contact
*Correspondence: yulongli@pku.edu.cn
https://doi.org/10.1016/j.neuron.2023.02.024

SUMMARY

Histamine (HA) is a key biogenic monoamine involved in a wide range of physiological and pathological processes in both the central and peripheral nervous systems. Because the ability to directly measure extracellular HA in real time will provide important insights into the functional role of HA in complex circuits under a variety of conditions, we developed a series of genetically encoded G-protein-coupled receptor-activation-based (GRAB) HA (GRAB$_{HA}$) sensors with good photostability, sub-second kinetics, nanomolar affinity, and high specificity. Using these GRAB$_{HA}$ sensors, we measured electrical-stimulation-evoked HA release in acute brain slices with high spatiotemporal resolution. Moreover, we recorded HA release in the preoptic area of the hypothalamus and prefrontal cortex during the sleep-wake cycle in freely moving mice, finding distinct patterns of HA dynamics between these specific brain regions. Thus, GRAB$_{HA}$ sensors are robust tools for measuring extracellular HA transmission in both physiological and pathological processes.

INTRODUCTION

The biogenic amine histamine (HA) is an important signaling molecule in the immune, digestive, and nervous systems. For example, HA is secreted by basophils and mast cells as part of a localized immune response, playing a role in allergy and itch.[1] HA is also released by enterochromaffin-like cells in the stomach, triggering the release of stomach acids.[2] Since the discovery that antihistamines also have sedative properties, the role of HA in the central nervous system has attracted considerable attention.[3] In the vertebrate brain, HA is synthesized primarily in the tuberomammillary nucleus (TMN) in the posterior hypothalamus,[4] and histaminergic TMN neurons project throughout the brain, regulating various functions, such as the sleep-wake cycle, feeding, attention, and learning.[5]

Despite its clearly important role in a wide range of physiological and pathological processes, the spatiotemporal dynamics of HA release during various behaviors remain poorly understood due in large part to the limitations associated with current detection methods. For example, microdialysis combined with analytical techniques has been widely used to measure the dynamics of HA release in the living brain.[6] However, microdialysis often has low temporal resolution due to the relatively long time needed to collect the samples. In addition, complementary approaches using electrochemical methods such as fast-scan cyclic voltammetry have been developed for detecting HA in real time.[7] However, both microdialysis and electrochemical methods have limited spatial precision and lack cell-type specificity. Coupling diamine oxidase with an optical oxygen nanosensor can provide continuous tracking of HA concentration,[8] but the nanosensor has low sensitivity (with a lower limit of detection of approximately 1.1 mM) and specificity and is less effective at detecting HA in deep brain regions. The Tango-Trace strategy can be used to detect HA release *in vivo* with a high signal-to-background ratio by coupling the β-arrestin signaling pathway to the expression of a reporter gene.[9–11] However, this approach requires several hours to express the fluorescent reporter protein and cannot be used to monitor the rapid dynamics of HA-mediated transmission. Finally, conformational H_1R and H_3R sensors based on both fluorescence resonance energy transfer (FRET) and bioluminescence resonance energy transfer (BRET) have been developed to measure their interaction with HA (and

mechanical force or other H_3R ligands, respectively),[12–14] but they generally have a low signal-to-noise ratio and a low dynamic range, thus strongly limiting their ability to monitor HA release *in vivo*.

Recently, building on the successful G-protein-coupled receptor-activation-based (GRAB) strategy, our group and others independently developed a series of genetically encoded sensors for detecting a variety of neurotransmitters and neuromodulators with high sensitivity, selectivity, and spatiotemporal resolution in *in vivo* preparations.[15–19] Using this strategy, we developed a pair of genetically encoded fluorescent sensors called $GRAB_{HA1h}$ and $GRAB_{HA1m}$ (abbreviated here as HA1h and HA1m, respectively), based on the human H_4R and water bear (tardigrade) H_1R receptors, respectively, to measure extracellular HA with high sensitivity and high spatiotemporal resolution, both *in vitro* and *in vivo*. These sensors have high specificity for HA, rapid kinetics (in the order of sub-seconds), and an increase in fluorescence of 300%–500% in response to HA when applied *in vitro*. Using these novel HA sensors, we monitored the release of endogenous HA during the sleep-wake cycle in freely moving mice and found distinct patterns of HA dynamics between two specific brain regions. Thus, these genetically encoded sensors can be used to gain important new insights into the dynamic properties of HA signaling under both physiological and pathological conditions.

RESULTS

Development and characterization of GRAB sensors for detecting histamine

To monitor the change in extracellular HA levels with high spatial and temporal resolution, we designed a genetically encoded GRAB sensor based on HA receptors (Figure 1A). First, we systematically screened a series of G-protein-coupled HA receptors, including human H_1R, H_2R, H_3R, and H_4R (Figures S1A and S1B). The third intracellular loop (ICL3) in the HA receptors was replaced with a circularly permutated EGFP (cpEGFP) and ICL3 derived from the previously developed and characterized $GRAB_{NE}$ norepinephrine sensor.[20] We selected the hH_4R-based chimera, which has good plasma membrane trafficking (Figure S1B), for further optimization. We then optimized the length and amino acid composition of the linker region near the insertion site, as well as critical residues in cpEGFP based on our previous experience[15,17,21–24] in developing GRAB sensors (Figures 1B, S2A1, and S3C). Screening more than 2,000 sensor variants identified the sensor with the highest fluorescence response (see STAR Methods for details), which we called HA1h (Figures 1B, S2A2, and S3A). When expressed in cultured HEK293T cells, HA1h trafficked to the plasma membrane and produced a peak change in fluorescence ($\Delta F/F_0$) of ~370% in response to the extracellular application of 10 μM HA (Figures 1F–1I). We also generated an HA-insensitive form of this sensor, which we call HA1mut, by introducing an E211A substitution in hH_4R (Figures 1B, S2A1, and S3A). HA application induced a dose-dependent increase in fluorescence in HA1h-expressing HEK293T cells, with a half-maximal effective concentration (EC_{50}) of 17 nM (Figure 1J). Consistently, a similar binding affinity (K_d) of 13 nM was obtained for the binding of [³H]HA to

HA1h in a radioligand binding assay (Figure S7A). We also sought to develop a HA sensor with a larger dynamic range by screening HA receptors obtained from 11 species in which we grafted the ICL3-cpEGFP module from the HA1h sensor (Figures 1C and 1D). Based on the results of this screening, we selected the chimera with the highest response, namely HA0.5m, based on the water bear (tardigrade) H_1R for further ICL3 replacement, amino acid composition of the linker region, and cpEGFP optimization (Figure S2B; see STAR Methods for details), yielding a high-response sensor we call HA1m (Figures 1E and S3B), which produces an ~590% increase in fluorescence upon application of 100 μM HA (Figures 1F–1I) and an EC_{50} of 380 nM when expressed in HEK293T cells (Figure 1J). The affinities of HA receptor subtypes vary from nanomolar to micromolar (Figure S1A). HA sensors, including high-affinity version HA1h and medium-affinity version HA1m, provide a powerful toolbox to detect HA release over a broad range of concentrations.

We then characterized the plasma membrane trafficking, kinetic properties, wavelength spectrum, and photostability of the HA sensors in cultured HEK293T cells. When expressed in HEK293T cells, HA1h, HA1m, and HA1mut sensors trafficked to the cell membrane, indicated by their high colocalization ratio with membrane-targeted RFP (Figure S1D). Using a local perfusion system and high-speed line-scanning, both HA1h and HA1m had a rapid increase in fluorescence in response to a saturating concentration of HA, with an on-rate (time constant) of 0.6 and 0.3 s, respectively (Figures 2A–2C). The off-rate of HA1h and HA1m was measured by rapidly applying H_4R and H_1R antagonists, respectively, yielding an off-rate (time constant) of 2.3 s (HA1h) and 1.4 s (HA1m) (Figures 2A–2C). Both HA1h and HA1m had a similar spectrum as EGFP, with an excitation peak at ~505 nm and an emission peak at ~520 nm under one-photon illumination, and an excitation peak at ~920 nm under two-photon illumination (Figure S4A). HA1h and HA1m showed better or comparable photostability than EGFP under confocal laser illumination in cultured HEK293T cells (Figures S5A–S5C). During wide-field LED illumination, a superior photostable GFP, namely StayGold,[25] showed more photostability than HA1h and HA1m sensors (Figures S5D–S5F).

Next, we tested whether our HA sensors could trigger downstream signaling pathways, including G-protein-dependent and/or β-arrestin-dependent pathways. Because human H_4R (hH_4R) is a Gi-coupled G-protein-coupled receptor (GPCR), we used a chimeric $G\alpha_{q-i}$ protein, which switches the downstream response from Gi to Gq signaling.[26,27] Using intracellular Ca^{2+} imaging, we found that the hH_4Rs and water bear H_1Rs (wbH_1Rs) signaled robustly, whereas both the HA1h and HA1m sensors produced virtually no response (Figure 2D). Similar results were obtained when we measured signaling via the β-arrestin pathway using the Tango assay (Figure 2E). Furthermore, consistent with our Tango assay results, we found that exposing HA1h- and HA1m-expressing cultured neurons to a saturating concentration of HA for 3 h led to virtually no internalization of either sensor (Figures S6A and S6B). Taken together, these results suggest that our HA sensors can be used to measure extracellular HA without inadvertently activating downstream signaling pathways.

To measure the performance of our HA sensors in a more physiologically relevant context, we expressed HA1h, HA1m, or
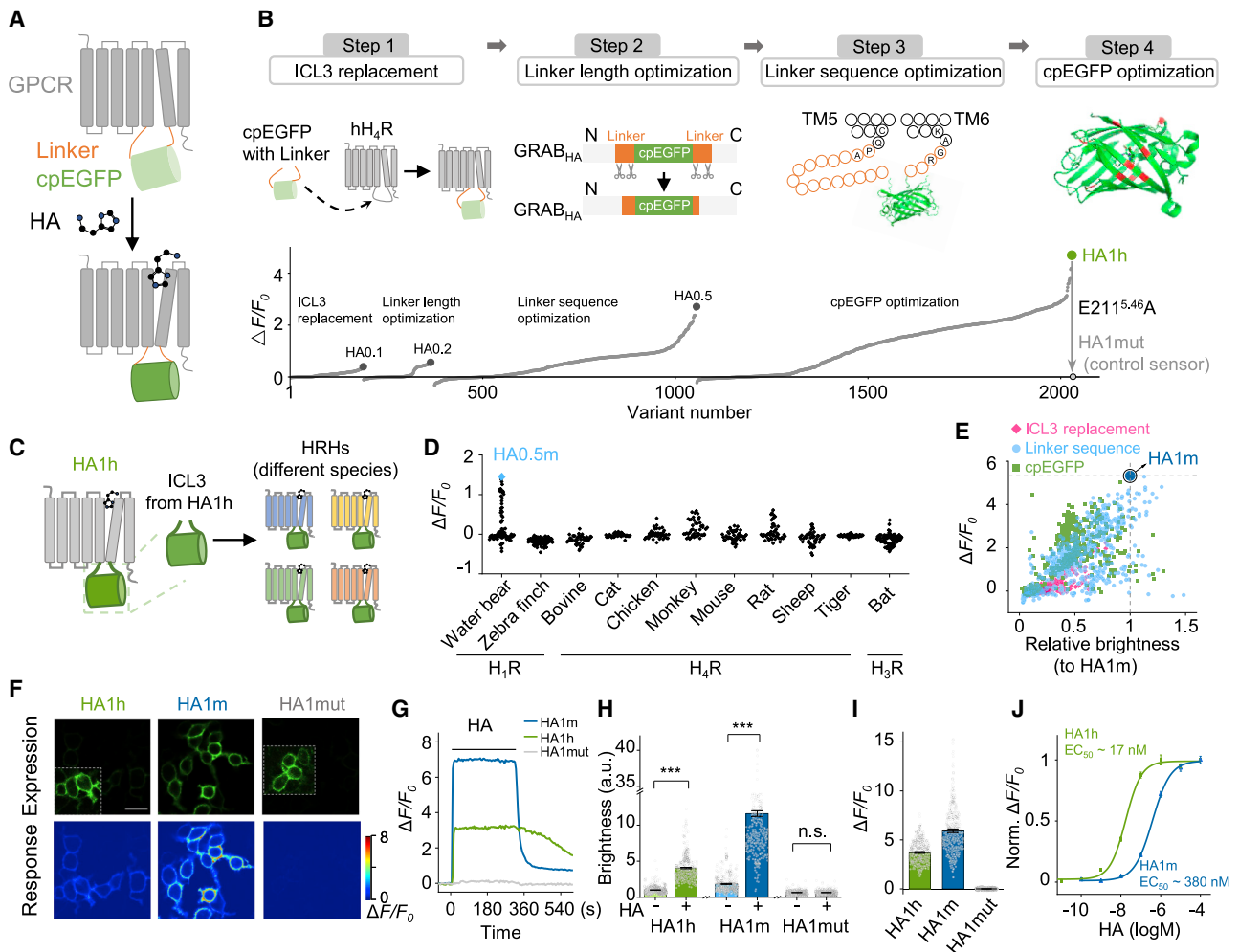
CellPress

Figure 1. Development of genetically encoded fluorescent GRAB_HA sensors

(A) Schematic depiction of the principle behind the GRAB_HA sensors in which cpEGFP is inserted within the ICL3 of the HA receptor. Upon binding HA, the resulting conformational change causes an increase in fluorescence.

(B) Steps used to identify the most responsive candidate HA sensors based on the human H_4R and GRAB_NE ICL3, by screening the ICL3 insertion sites, the linker length, and key residues in the linker and cpEGFP. Shown is the final HA1h sensor used in this study, as well as the corresponding HA1mut sensor used in this study as a negative control.

(C) Schematic depiction of the principle used to generate and screen GRAB_HA sensors derived from other species' HA receptors (HRHs).

(D) Further development of HA sensors by screening H1, H3, and H4 receptors obtained from the indicated species.

(E) Optimization of candidate HA sensors based on the water bear (tardigrade) H_1R.

(F–J) Characterization of the expression and performance of the HA1h, HA1m, and HA1mut sensors expressed in HEK293T cells, showing membrane trafficking (F), representative time courses (G), relative brightness (H), peak response to HA (I), and apparent affinity (J). The dashed box in (F) shows the image with enhanced contrast. Scale bars, 50 μm. n = 400 cells from 4 wells for different groups in (H) and (I). n = 3 wells in (J). Data are shown as mean ± SEM in (H)–(J) with the error bars or shaded regions indicating the SEM, *** p < 0.001; n.s., not significant.

See also Figures S1–S3.

HA1mut in cultured rat cortical neurons using an adeno-associated virus (AAV). We found that HA1h and HA1m localize throughout the neuronal plasma membrane (Figure 2F). Moreover, bath application of a saturating concentration of HA caused a robust increase in both HA1h and HA1m fluorescence (with peak $\Delta F/F_0$ values of approximately 180% and 320%, respectively), with no measurable effect on HA1mut (Figures 2G and 2H). In addition, similar to our results obtained with HEK293T cells, we found that neurons expressing either HA1h or HA1m

had a dose-dependent increase in fluorescence, with EC_{50} values of 19 and 400 nM, respectively (Figure 2I). To confirm the specificity of our sensors for HA, we tested the effects of an HA precursor, several HA metabolites, and several monoamines and neurotransmitters, finding no measurable response to any of these compounds (Figure 2J). Notably, the HA-induced responses in HA1h and HA1m were fully blocked by the H_4R antagonist JNJ-7777120 and the H_1R antagonist clemastine, respectively, while all other HA receptor antagonists had no effect
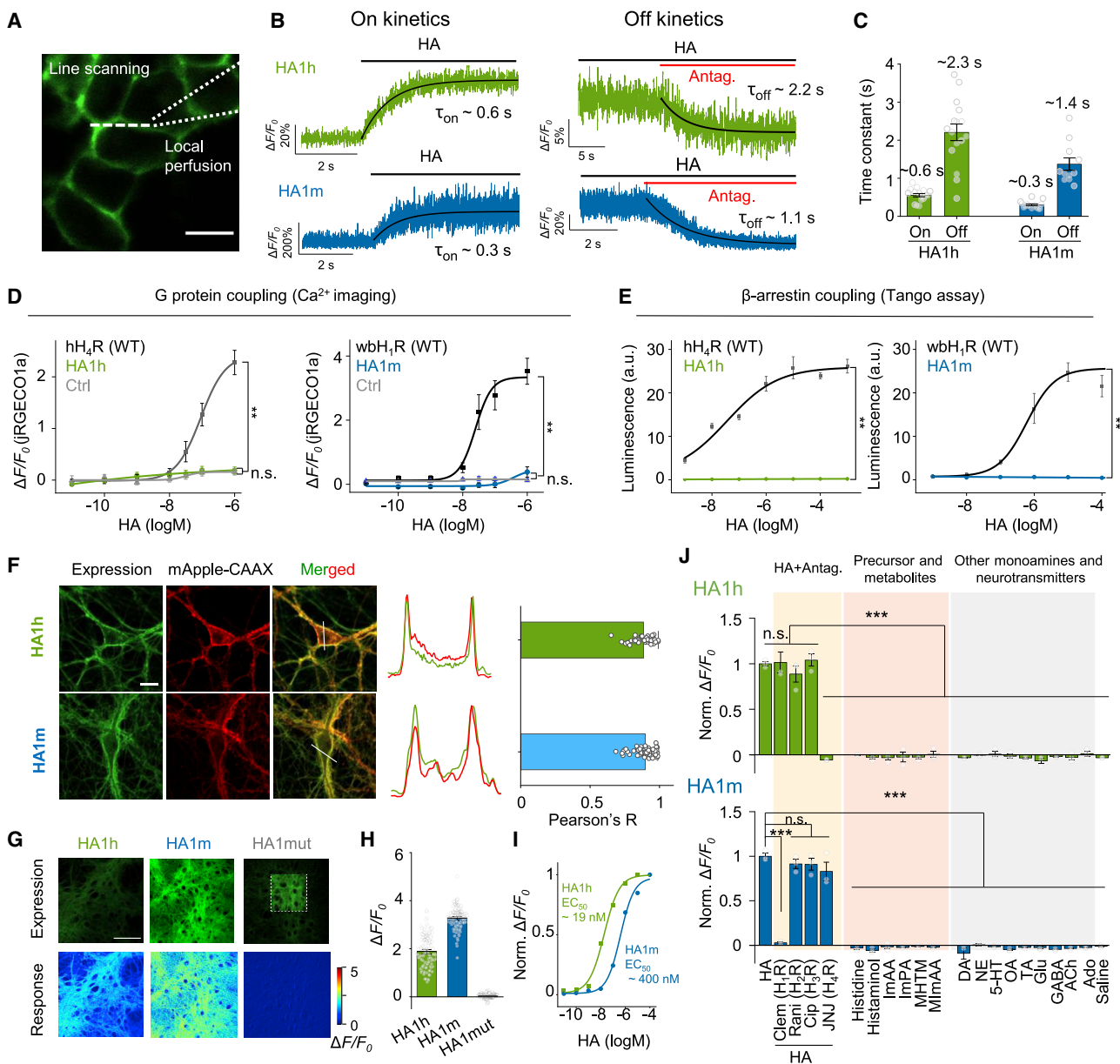
Figure 2. Characterization of GRAB$_{HA}$ sensors in HEK293T cells and cultured rat cortical neurons

(A–C) Measurement of the kinetics of HA1h and HA1m expressed in HEK293T cells. HA was applied to cells expressing either HA1h or HA1m to measure τ_{on}. The appropriate antagonist (100 μM JNJ-7777120 for HA1h and 100 μM clemastine for HA1m) was then applied in the continued presence of HA to measure τ_{off}. Representative traces (B) and summary results (C) are shown; the white dashed line in (A) indicates the line-scanning region. n ≥ 10 cells from 4 to 5 cultures. Scale bars, 50 μm.

(D and E) G-protein (D) and β-arrestin (E) coupling were measured in cells expressing HA1h (or hH$_4$R as a positive control) or HA1m (or wbH$_1$R as a positive control) using Ca^{2+} imaging (D) and a Tango assay (E). ** p < 0.01; n.s., not significant. n = 3 wells for different groups.

(F) Analysis of fluorescence and membrane trafficking of the HA1h and HA1m sensors expressed in cultured rat cortical neurons. Membrane-targeted mApple (mApple-CAAX) was co-expressed to label the plasma membrane. Left: fluorescence images of cultured neurons expressing the indicated HA sensors (green) and mApple (red). Middle: normalized line-scanning plots of the fluorescence signals measured in both the green and red channels. Right: a summary of Pearson's correlation measured between the indicated HA sensor and mApple-CAAX; n = 45 neurons for HA1h, 63 neurons for HA1m from 3 coverslips for different groups. Scale bars, 20 μm.

(G–I) Characterization of the representative responses (G), peak response to HA (H), and apparent affinity (I) of the HA1h, HA1m, and HA1mut sensors expressed in cultured rat cortical neurons. Scale bars: 100 μm in (G). n = 115, 108, and 108 neurons from 3 wells for HA1h, HA1m, and HA1mut in (H), respectively.

(J) Summary of the normalized fluorescence change measured in cultured rat cortical neurons expressing HA1h (top panel) or HA1m (bottom panel) in response to HA alone, HA applied together with the indicated HA receptor antagonist, HA precursor, metabolites, and the indicated neurotransmitters (all compounds were applied at 5 μM). Clem, clemastine; Rani, ranitidine; Cip, ciproxifan; JNJ, JNJ-7777120; ImAA, imidazoleacetic acid; ImPA, imidazolepyruvic acid; MHTM,

(legend continued on next page)

Neuron
NeuroResource

CellPress

(Figure 2J) on cultured neurons. Consistent with the results in cultured neurons, the HA-induced responses in HA1h and HA1m of HEK293T cells were specifically blocked by the H$_4$R antagonist and the H$_1$R antagonist (Figure S4B), respectively. Furthermore, a radioligand binding assay was performed to test whether HA sensors specifically are bound by HA. We found HA and the H$_4$R agonist N^α-methylhistamine to specifically bind to the HA1h sensor, while HA precursor and HA metabolites, and several monoamines and neurotransmitters, had no measurable binding (Figure S7B). Together, these results indicate that both HA1h and HA1m retain the pharmacological profile and ligand specificity of their corresponding parent receptors.

GRAB$_{HA}$ sensors can be used to image HA release in acute mouse brain slices

Next, we examined whether our HA sensors could be used to detect the release of endogenous HA. We therefore injected an AAV expressing HA1m under the control of the human synapsin (hSyn) promoter into the mouse prefrontal cortex (PFC) and prepared acute brain slices 2–3 weeks later (Figures 3A and 3B). We found that applying electrical stimuli at 20 Hz elicited a pulse-number-dependent increase in HA1m fluorescence that was blocked by treating the slices with the H$_1$R antagonist clemastine (Figures 3C and 3D). We also measured the kinetics of the response to 10, 20, 50, and 100 pulses delivered at 20 Hz and obtained rise time constants (τ_{on}) and decay time constants (τ_{off}) of 1.4–5.2 and 10–13 s, respectively (Figure 3E). Interestingly, we also found that the HA1m signal increased at the site of stimulation and then propagated outward (Figures 3F–3H). To test the maximum response of HA1m in acute brain slices, we applied 10 μM HA and obtained a robust fluorescence increase (~400%), which was abolished by the application of clemastine (Figures 3I and 3J). Thus, our HA1m sensor can detect the release of endogenous HA with high spatiotemporal resolution.

GRAB$_{HA}$ sensors can be used to measure HA release *in vivo*

A wealth of pharmacological and genetic data has shown that HA plays an essential role in regulating the sleep-wake cycle.[28] Thus, based on these findings, we examined whether our HA sensors could be used to measure histaminergic activity during the physiological sleep-wake cycle, focusing on the transitions between sleep-wake states. In the mammalian brain, the preoptic area (POA) regulates sleep and receives extensive projections from histaminergic neurons.[29,30] We expressed the HA1m sensor in the POA and then performed simultaneous fiber photometry, electroencephalography (EEG), and electromyography (EMG) recordings in freely behaving mice (Figure 4A). We found that the signal produced by the HA1m sensor in the POA was relatively high when the mouse was awake compared with the signal measured during both rapid eye movement (REM) and non-REM (NREM) sleep (Figures 4B and 4C), supporting previously reported data obtained using microdialysis.[31] As a

control, we also expressed the HA1m sensor in the POA of histidine decarboxylase knockout (HDC KO) mice and found no significant change in HA1m fluorescence at any stage during the sleep-wake cycle (Figures 4D and 4E). Because our HA sensors have rapid kinetics, we then calculated the change in HA1m signal at the transitions between various sleep states and found that the signal increased during the REM → wake and NREM → wake transitions but decreased during the wake → NREM and NREM → REM transitions (Figure 4F).

We recorded HA release in the POA using our medium-affinity HA1m sensor, as the POA receives a relatively dense number of histaminergic projections. Next, we examined whether we could measure HA release in the PFC, a brain region that receives a more moderate density of histaminergic projections and plays a critical role in regulating executive functions such as attention and decision, functions that are based on wakefulness. To account for the lower density of histaminergic projections, we expressed the high-affinity HA1h sensor in the PFC and performed simultaneous fiber photometry, EEG, and EMG recordings in freely behaving mice (Figure 5A). Similar to our results obtained using the HA1m sensor expressed in the POA, we found that the HA1h signal in the PFC was higher when the animal was awake compared with during both REM and NREM sleep (Figures 5B and 5C), again consistent with previously reported microdialysis data.[32] As expected, consistent with our *in vitro* results, an i.p. injection of the H$_4$R antagonist JNJ-7777120 virtually eliminated fluorescence of the HA1h sensor expressed in the PFC, even when the mouse was awake (Figures 5D and 5E). Furthermore, no significant change in fluorescence was measured in the PFC of mice expressing the mutant HA1mut sensor at any time during the sleep-wake cycle (Figures 5F and 5G). Finally, no significant attenuation in HA1h sensor signals was recorded over 1 day under low-excitation light intensity and sample rate (Figures S9A–S9C).

HA is believed to play an important role in both the initiation and maintenance of wakefulness.[28] Thus, the HA H3 receptor H$_3$R is a novel promising target for improving vigilance, and the H$_3$R antagonist ciproxifan may have potential therapeutic benefits in the context of vigilance deficiency.[33] In addition, the stimulant caffeine is widely used to maintain wakefulness. We therefore used our HA sensors to determine whether ciproxifan and/or caffeine mediate their effects on wakefulness by increasing HA release (Figure 5H). As expected, we found that both ciproxifan and caffeine prolonged wakefulness in mice (Figures 5I and 5J). Interestingly, however, we found that ciproxifan—but not caffeine—increased the fluorescence signal of HA1h expressed in the PFC (Figures 5I–5K and S8A–S8C). we further confirm that ciproxifan also increased the fluorescence signal of HA1m expressed in POA in wild-type mice but not HDC KO mice (Figures S8D–S8F). These results indicate that although both ciproxifan and caffeine promote wakefulness, they do so via distinct mechanisms, with ciproxifan, but not caffeine, increasing HA release in the PFC.

1-methylhistamine; MImAA, methylimizoleacetic acid; DA, dopamine; NE, norepinephrine; 5-HT, serotonin; OA, octopamine; TA, tyramine; Glu, glutamate; GABA, γ-aminobutyric acid; Ach, acetylcholine; Ado, adenosine. n = 3 coverslips for each group. Paired two-tailed Student's t tests were performed. ** p < 0.01; n.s., not significant. Data are shown as mean ± SEM.
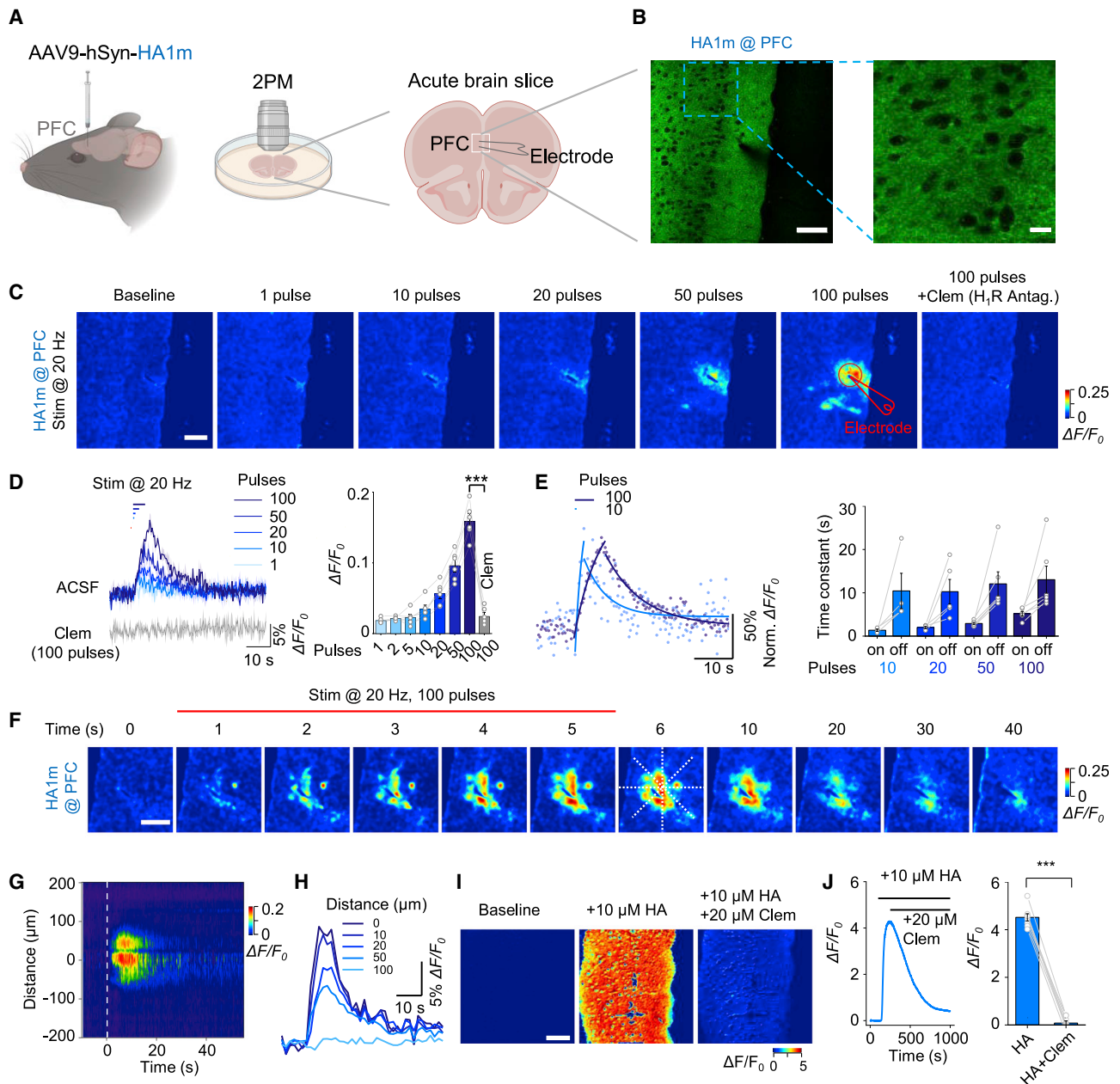See also Figures S4–S7.

Figure 3. Using the GRAB$_{HA}$ sensor to measure the release of endogenous HA in acute mouse brain slices

(A) Schematic illustration of the acute mouse brain slice experiments. An AAV expressing hSyn-HA1m was injected into the PFC region; acute brain slices (coronal slices containing the PFC) were then prepared and used for electrical stimulation experiments.

(B) Exemplar two-photon microscopy images showing HA1m expressed in the PFC. Scale bars: 100 μm (left) and 20 μm (right).

(C) Representative pseudocolor images showing the corresponding fluorescence change in HA1m-expressing slices in response to 1, 10, 20, 50, and 100 pulses delivered at 20 Hz in ACSF, and in response to 100 pulses in the presence of the H$_1$R antagonist clemastine (20 μM). Scale bars, 100 μm.

(D) Exemplar traces (left) and summary of the peak fluorescence change (right) measured in HA1m-expressing slices stimulated as indicated. Where indicated, clemastine (Clem) was applied at 20 μM. n = 6 slices from 4 mice. *** p < 0.001.

(E) Representative trace with fitted curves (left) and summary data of the on-time and off-time constants (right), measured for the change in HA1m fluorescence in response to the indicated number of pulses applied at 20 Hz. n = 4, 5, 6, and 6 slices from 3, 3, 4, and 4 mice for 10, 20, 50, and 100 pulses, respectively.

(F) Exemplar time-lapse pseudocolor images of HA1m fluorescence in response to 100 pulses at 20 Hz applied during the first 5 s. The dashed lines were used to analyze spatial dynamics in (G) and (H). Scale bars, 100 μm.

(G) Spatial profile of the evoked change in fluorescence shown in (F); the vertical dashed line at time 0 indicates the start of the stimulation.

(H) Temporal dynamics of the change in HA1m fluorescence as shown in (G), measured 10, 20, 50, and 100 μm from the release center.

(I) Example expression and pseudocolor images before and after application of 10 μM HA and H$_1$R antagonist clemastine (Clem). Scale bars represent 100 μm.

(J) Example trace and grouped peak response data. n = 8 slices from 4 mice. *** p < 0.001.
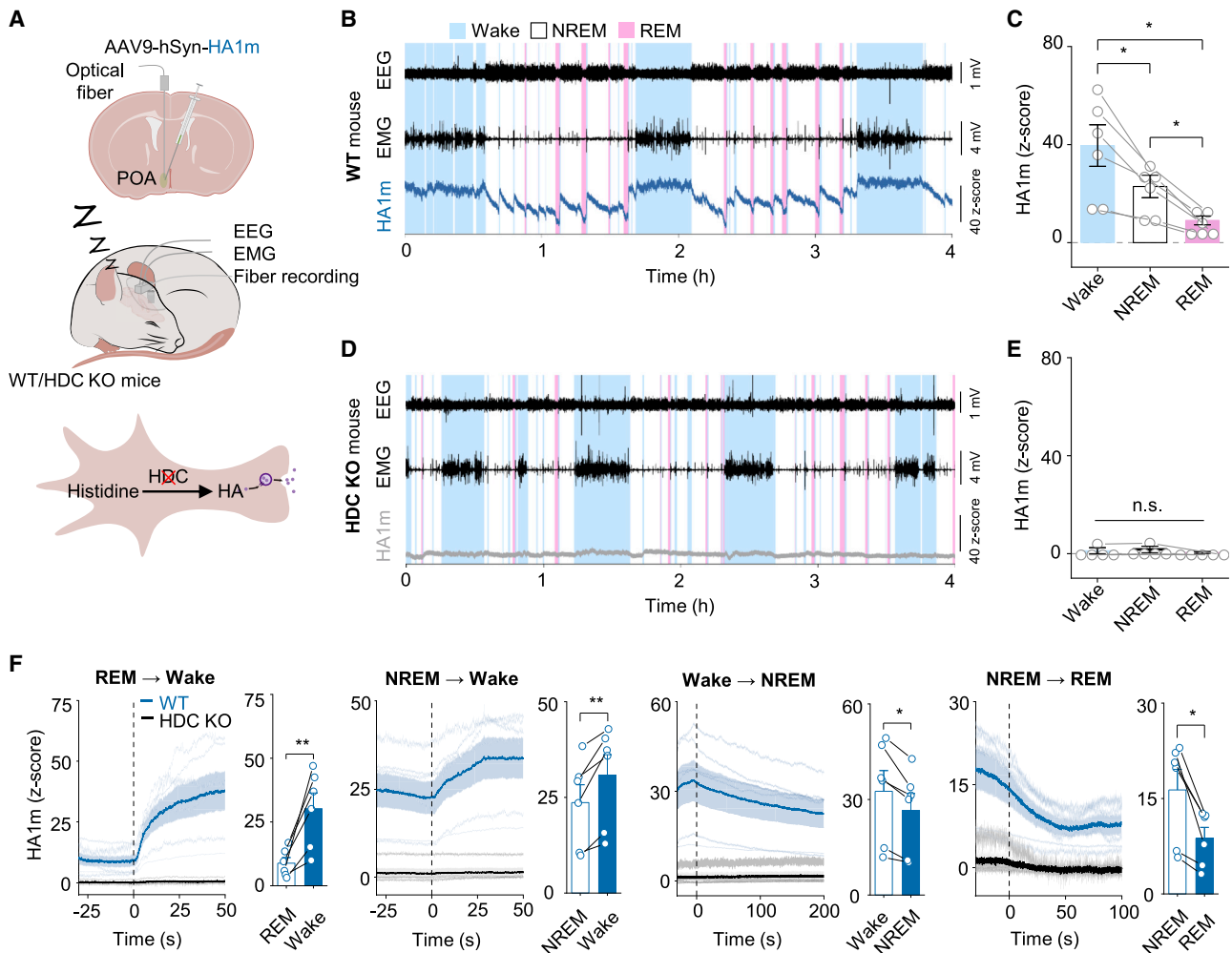
Figure 4. Using the GRAB_HA1m sensor to measure *in vivo* HA release in the POA during the sleep-wake cycle in freely moving mice

(A) Schematic diagram depicting the strategy for fiber photometry recording of HA1m fluorescence in the POA of freely behaving wild-type (WT) and histidine decarboxylase knockout (HDC KO) mice during the sleep-wake cycle. Top panel, an AAV expressing hSyn-HA1m was injected into the PFC region; middle panel, schematic diagram depicting fiber photometry recording of HA1m signals, EEG, and EMG. Bottom panel, HA synthesis process.

(B and D) Example traces of simultaneous EEG, EMG, and HA1m recordings in a WT (B) and HDC KO (D) mouse. In this and subsequent figures, the wake state is shaded in blue, REM sleep is shaded in pink, and NREM sleep is unshaded.

(C and E) Summary of the average HA1m fluorescence measured in WT (C; n = 6 mice) and HDC KO mice (E; n = 5 mice) in the indicated sleep-wake states. Each symbol represents the recording from one mouse.

(C) One-way ANOVA: F = 16.3913, p = 0.0007; Tukey's post hoc test: wake vs. NREM p = 0.0335, wake vs. REM p = 0.0207, NREM vs. REM p = 0.0153; * p < 0.05.

(E) One-way ANOVA: F = 1.2401, p = 0.3308; n.s., not significant.

(F) Time course and average signals measured for the HA1m sensor during the indicated transitions between sleep-wake states. The vertical dashed lines at time 0 represent the transition time. paired t test, REM → wake t = 4.2803, p = 0.0079; NREM → wake t = 4.0586, p = 0.0097; wake → NREM t = 3.7418, p = 0.0134; NREM → REM t = 3.9835, p = 0.0105; * p < 0.05, ** p < 0.01.

Data are shown as mean ± SEM. In (C), (E), and (F), the error bars or shaded regions indicate the SEM. In (F), the bold lines indicate the mean trace of all mice. See also Figure S8.

The kinetics of HA release differ in different brain regions

Histaminergic neurons send their projections to numerous target regions throughout the brain.[29] We therefore asked whether the temporal pattern of HA release is universal throughout the brain or differs among various brain regions. As a first step toward addressing this question, we expressed the HA1h sensor in both the PFC and POA and then simultaneously recorded the fluorescence signals in these two nuclei (Figure 6A). We found that the magnitude of the HA1h signal measured at each state in the sleep-wake cycle was similar between the PFC and POA (Figures 6B and 6C). We also found a close temporal cross-correlation in the time-shift data (Figure 6D), indicating that the signal change in the POA preceded the signal change in the PFC. We then aligned and normalized the signals measured during the wake-sleep state transitions and found that the signals measured
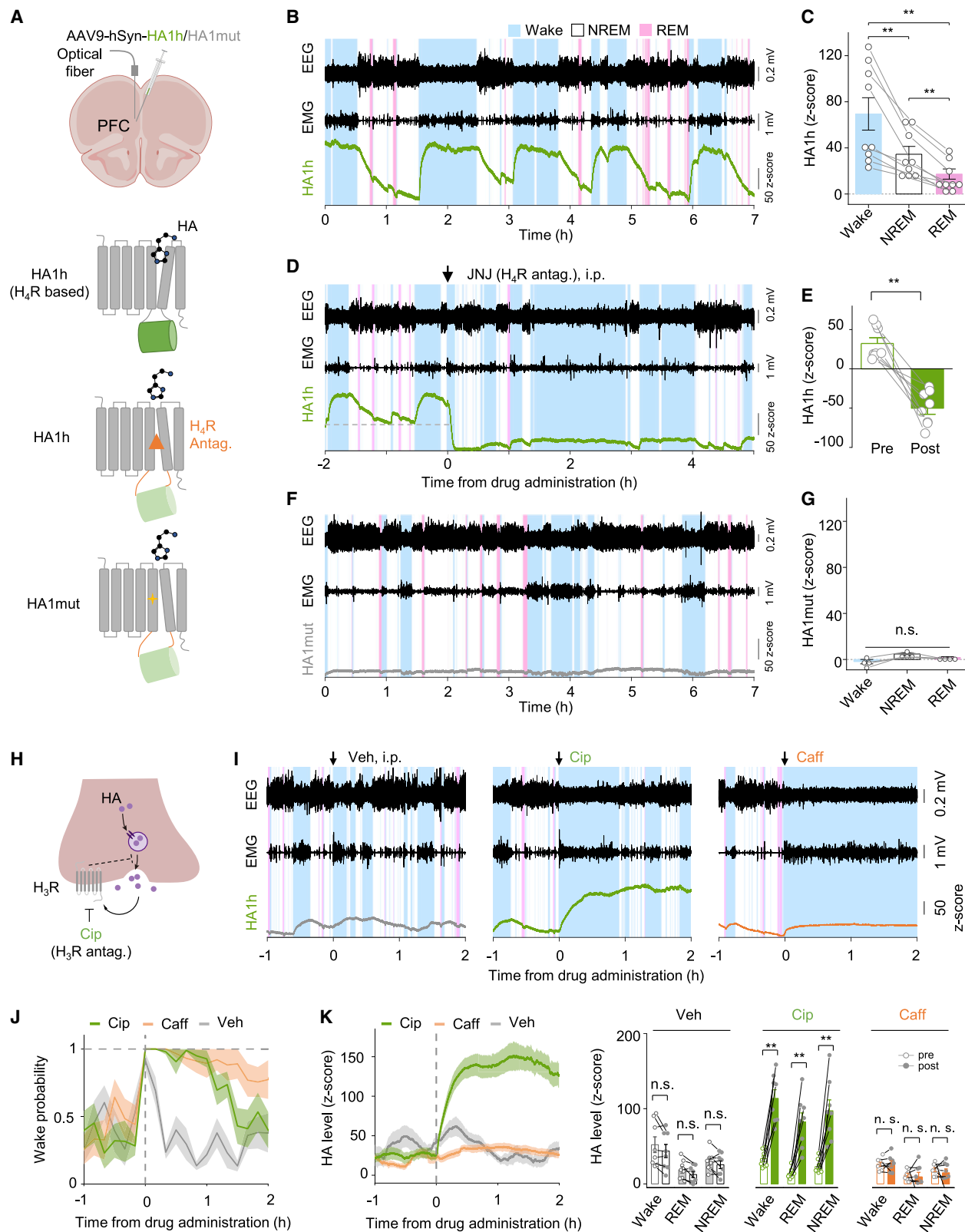
(legend on next page)

in the POA were faster than the corresponding signals measured in the PFC during both the REM → wake transition, the NREM → wake transition, and the wake → NREM transition (Figure 6E). We also quantified the kinetics of the responses by calculating the t_{50} value of the signal rise or fall at each transition. We found that the t_{50} values measured in the POA were significantly lower than the corresponding values measured in the PFC during the REM → wake, NREM → wake, and wake → NREM transitions, but were similar during the NREM → REM transition (Figure 6F), indicating a clear difference in HA release kinetics between the POA and PFC (summarized schematically in Figure 6G). These results raise at least two possibilities: first, histaminergic projections in the POA and PFC may arise from different subpopulations of histaminergic neurons; alternatively, HA release may be modulated by other neurotransmitters and modulators acting locally at the site of histaminergic innervation (Figure S10).

DISCUSSION

Here, we report the development and characterization of two genetically encoded GPCR-activation-based fluorescent sensors for measuring changes in extracellular HA in real time. With their high sensitivity, high selectivity, and rapid kinetics, GRAB$_{HA}$ sensors can reliably detect endogenous HA release both *in vitro* and in freely behaving animals under physiological conditions.

Our GRAB$_{HA}$ sensors offer several clear advantages over existing methods for measuring HA. First, GRAB$_{HA}$ sensors have high sensitivity and a relatively high signal-to-noise ratio in response to HA. Specifically, the HA1h and HA1m sensors produce a peak fluorescence response of ∼300% and 500%, respectively, with an apparent affinity of ∼20 and 400 nM, respectively. In contrast, GPCR-based FRET[12] and BRET[13] probes for detecting HA have a low peak response and are limited to use in *in vitro* applications. Second, our GRAB$_{HA}$ sensors have rapid kinetics, with rise and decay times of 0.3–0.6 and 1.4–2.3 s, respectively. Although this response time of GRAB$_{HA}$ sensors is slightly longer than fast-scan cyclic voltammetry, it is sufficient to report physiologically relevant changes in HA

levels and is similar to the response times reported for wild-type GPCRs[34] and other GRAB sensors.[16,20,23] In addition, our GRAB$_{HA}$ sensors have high spatial resolution and are photostable, allowing for stable recordings over prolonged experiments. Finally, our sensors have high specificity for HA, as they can reliably detect changes in extracellular HA in wild-type mice, but produce no signal in KO mice lacking the enzyme HDC. Building on these key advantages over other tools, we used our GRAB$_{HA}$ sensors to measure the HA release with high spatial resolution in acute brain slices by combining the sensor with two-photon imaging. In addition, we combined our sensors with fiber photometry recording to monitor real-time changes in histaminergic activity in the mouse brain during the sleep-wake cycle.

Our GRAB$_{HA}$ sensors have the same high specificity for HA and pharmacological profile of their corresponding parent receptors. Using cultured neurons, we found that both the human and tardigrade receptor-derived HA sensors respond to HA, but do not respond to an HA precursor, HA metabolites, or any other neurotransmitters tested. Similarly, each sensor's signal was blocked by the corresponding receptor antagonists, but was unaffected by other HA receptor antagonists, indicating that the complementary pharmacological profile of these two HA sensors can be exploited to study how HA release is regulated by various compounds that target histaminergic signaling. For example, the H$_3$R receptor is a promising new target for improving vigilance, and an H$_3$R antagonist has been shown to increase HA turnover by blocking the negative feedback regulation of HA release (see Figure 5H).[35,36] Consistent with these previous studies, we found that the GRAB$_{HA}$ response was larger in wild-type mice that received an H$_3$R antagonist, but was not affected in HDC-deficient mice (see Figures S6D–S6F), indicating that our HA sensors can be used to monitor the effects of H$_3$R antagonists on histaminergic signaling.

Using our GRAB$_{HA}$ sensor, we also found that specific brain regions have distinct patterns of HA release kinetics. This finding suggests that the projections of histaminergic neurons are heterogeneous; however, another possibility is that HA release may be modulated to some extent by local or regional neurotransmitters,

Figure 5. Using the GRAB$_{HA1h}$ sensor to measure HA release in the PFC in freely moving mice during the sleep-wake cycle

(A) Schematic diagram depicting the strategy for fiber photometry recording of HA1h or HA1mut fluorescence in the PFC of freely behaving mice during the sleep-wake cycle. Top panel, an AAV expressing either HA1h or HA1mut was injected into the PFC region and an optical fiber was implanted at the injection site. Bottom three panels, schematic diagram showing the responses of the HA1h and HA1mut sensors to HA, as well as the HA1h sensor in the presence of an H$_4$R antagonist.

(B and F) Example traces of simultaneous EEG, EMG, and HA1h (B) or HA1mut (F) recordings.

(C and G) Summary of the average HA1h (C) and HA1mut (G) fluorescence responses measured in the indicated sleep-wake states.

(C) n = 9 mice. One-way ANOVA: F = 21.7374, p = 0.0014; Tukey's post hoc test: wake vs. NREM p = 0.0074, wake vs. REM p = 0.0033, NREM vs. REM p = 0.0011; ** p < 0.01.

(G) n = 4 mice. One-way ANOVA: F = 9.5591, p = 0.0512; n.s., not significant.

(D) Example traces of simultaneous EEG, EMG, and HA1h recordings after an i.p. injection of the H$_4$R antagonist JNJ-7777120 (3 mg/kg body weight). The dashed line indicates the minimum level of HA1h signals before the antagonist is administrated.

(E) Summary of average HA1h fluorescence measured before (pre) and after (post) an injection of JNJ-7777120. n = 8 mice. Paired t test, t = 6.3859, p = 0.0004; ** p < 0.01.

(H) Schematic drawing depicting the effect of the H$_3$R antagonist, ciproxifan, on downstream HA release.

(I) Example traces of simultaneous EEG, EMG, and HA1h recordings in mice before and after administration of vehicle, ciproxifan (3 mg/kg body weight), or caffeine (15 mg/kg body weight).

(J) Time course of the probability of being in the awake state; the dashed line at time 0 indicates the administration of vehicle, ciproxifan, or caffeine.

(K) Time course (left) and average (right) HA1h signals measured in the PFC before and after administration of vehicle, ciproxifan, or caffeine. n = 8 mice. Two-way ANOVA between brain state and time; vehicle, F(time) = 3.9317, p = 0.0878; ciproxifan, F(time) = 57.1062, p = 0.0001, pre-post comparisons followed by Sidak's test, wake, NREM, and REM pre vs. post p < 0.0001; caffeine, F(time) = 0.1526, p = 0.7076; ** p < 0.01. n.s., not significant. Data are shown as mean ± SEM. See also Figures S8 and S9.
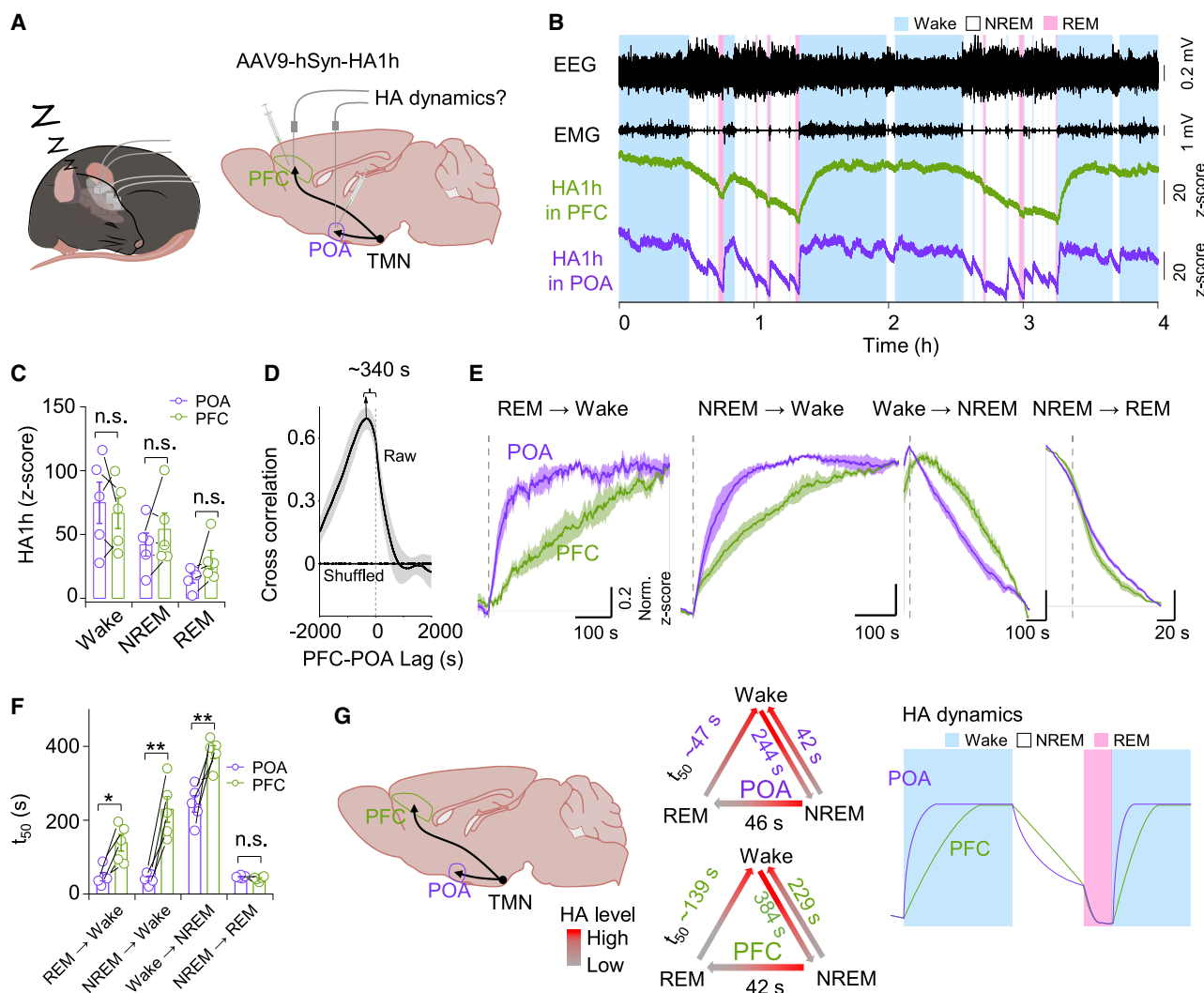
Figure 6. Simultaneously recording HA release in the mouse PFC and POA during the sleep-wake cycle reveals differences in kinetics

(A) Schematic diagram depicting the strategy for simultaneously recording HA1h fluorescence in the PFC and POA during the sleep-wake cycle in a freely moving mouse.

(B) Example traces of simultaneous EEG, EMG, and HA1h recordings in the PFC and POA.

(C) Summary of average HA1h fluorescence measured in the POA and PFC during the indicated sleep-wake states; n = 5 mice. Two-way ANOVA between brain state and nuclei, F(brain state) = 20.4065, p = 0.0007; F(nuclei) = 0.4091, p = 0.5572. n.s., not significant.

(D) Cross-correlation between the HA1h signals measured in the POA and PFC; as a control, the data were also shuffled and depicted as the horizontal line at y = 0. n = 5 mice.

(E) Time courses of the change in HA1h fluorescence measured in the POA and PFC at the indicated transitions between sleep-wake states. The vertical dashed lines represent the transition time.

(F) Summary of t_{50} measured for the change in HA1h fluorescence in the POA and PFC during the indicated sleep-wake state transitions. n = 5 mice. Two-way ANOVA between brain state transition and nuclei followed by Sidak's test, F(nuclei) = 52.4873, p = 0.0020. REM → wake, p = 0.0156; NREM → wake, p < 0.0001; wake → NREM, p = 0.0006; NREM → REM, p = 0.996; * p < 0.05, ** p < 0.01.

(G) Summary of the dynamics measured in the POA and PFC at the transitions between the various sleep-wake states.

Data are shown as mean ± SEM.

See also Figure S10.

modulators, and/or pathways (Figure S10). Alternatively, there is the possibility that the signals look slower when the reporters or sensors are located far from the release sites in certain brain region. In the brain, histaminergic projections: (1) originate from a single source, namely the TMN in the posterior hypothalamus; (2) innervate nearly all regions of the brain; and (3) regulate a wide range of behaviors and processes. Histaminergic TMN neurons are organized into five clusters, E1 through E5[37,38]; however, retrograde tracers injected into various brain regions labeled the entire TMN, without any clear topographical pattern.[37,39] To illustrate whether the projections of histaminergic neurons are heterogeneous, cell-type-specific labeling and whole-brain histaminergic

Neuron
NeuroResource

CellPress

axonal projection mapping are needed in future. With respect to the second possibility, several studies have shown that neurotransmitter release can be modulated at the level of the axon terminal. For example, dopamine release in the striatum is regulated at the axon terminal by acetylcholine.[40,41] Thus, HA release may also be modulated by the local environment, giving rise to our observation of heterogeneous release dynamics among target regions. Future studies combining our GRAB_HA sensors with other tools and strategies may shed new light on the mechanism underlying HA release and its regulation at the local and/or regional level.

In addition to regulating the sleep-wake cycle, HA plays a role in a number of physiological and pathological processes in the central nervous system, including feeding, motor control, cognition, narcolepsy, epilepsy, migraine, and Tourette's syndrome.[42,43] Interestingly, HA also serves as the primary neurotransmitter for visual input in *Drosophila* photoreceptors.[44,45] Moreover, HA plays a major role in allergic responses, including anaphylaxis.[1] Thus, this novel set of HA sensors suitable for both *in vitro* and *in vivo* applications can be used to measure HA release in a variety of settings and models, providing valuable new insights into the role of histaminergic signaling in both health and disease.

STAR★METHODS

Detailed methods are provided in the online version of this paper and include the following:

- KEY RESOURCES TABLE
- RESOURCE AVAILABILITY
  - Lead contact
  - Materials availability
  - Data and code availability
- EXPERIMENTAL MODEL AND SUBJECT DETAILS
  - Animals
  - Recombinant AAV
  - Cell lines
  - Primary cell cultures
- METHOD DETAILS
  - Molecular biology
  - Fluorescence imaging of cultured cells
  - Screening of GRAB_HA sensors
  - Spectra measurements
  - Photobleaching measurement
  - G_{qi} calcium imaging assay
  - Tango assay
  - [^{3}H]histamine competition binding assay
  - Two-photon fluorescence imaging of mouse acute brain slices
  - Surgery for virus injection, placement of EEG and EMG electrodes, and fiber implantation
  - Fiber photometry recording and analysis
  - Polysomnographic recording and analysis
- QUANTIFICATION AND STATISTICAL ANALYSIS

SUPPLEMENTAL INFORMATION

Supplemental information can be found online at https://doi.org/10.1016/j.neuron.2023.02.024.

AUTHOR CONTRIBUTIONS

DECLARATION OF INTERESTS

INCLUSION AND DIVERSITY

We support inclusive, diverse, and equitable conduct of research.

REFERENCES

1. White, M.V. (1990). The role of histamine in allergic diseases. J. Allergy Clin. Immunol. *86*, 599–605. https://doi.org/10.1016/s0091-6749(05)80223-4.

2. Prinz, C., Zanner, R., and Gratzl, M. (2003). Physiology of gastric enterochromaffin-like cells. Annu. Rev. Physiol. *65*, 371–382. https://doi.org/10.1146/annurev.physiol.65.092101.142205.

3. Faingold, C.L. (1978). Antihistaminics as central nervous system depressants. In Histamine II and Anti-histaminics, M. Rocha e Silva, ed. (Springer), pp. 561–573. https://doi.org/10.1007/978-3-642-66445-8_14.

4. Watanabe, T., Taguchi, Y., Hayashi, H., Tanaka, J., Shiosaka, S., Tohyama, M., Kubota, H., Terano, Y., and Wada, H. (1983). Evidence for the presence of a histaminergic neuron system in the rat brain: an immunohistochemical analysis. Neurosci. Lett. *39*, 249–254. https://doi.org/10.1016/0304-3940(83)90308-7.

5. Haas, H., and Panula, P. (2003). The role of histamine and the tuberomammillary nucleus in the nervous system. Nat. Rev. Neurosci. *4*, 121–130. https://doi.org/10.1038/nrn1034.

6. Yoshitake, T., Yamaguchi, M., Nohta, H., Ichinose, F., Yoshida, H., Yoshitake, S., Fuxe, K., and Kehr, J. (2003). Determination of histamine in microdialysis samples from rat brain by microbore column liquid chromatography following intramolecular excimer-forming derivatization with pyrene-labeling reagent. J. Neurosci. Methods *127*, 11–17. https://doi.org/10.1016/s0165-0270(03)00097-9.

7. Puthongkham, P., Lee, S.T., and Venton, B.J. (2019). Mechanism of histamine oxidation and electropolymerization at carbon electrodes. Anal. Chem. *91*, 8366–8373. https://doi.org/10.1021/acs.analchem.9b01178.

8. Cash, K.J., and Clark, H.A. (2013). Phosphorescent nanosensors for in vivo tracking of histamine levels. Anal. Chem. *85*, 6312–6318. https://doi.org/10.1021/ac400575u.

9. Barnea, G., Strapps, W., Herrada, G., Berman, Y., Ong, J., Kloss, B., Axel, R., and Lee, K.J. (2008). The genetic design of signaling cascades to record receptor activation. Proc. Natl. Acad. Sci. USA *105*, 64–69. https://doi.org/10.1073/pnas.0710487105.

10. Kroeze, W.K., Sassano, M.F., Huang, X.P., Lansu, K., McCorvy, J.D., Giguère, P.M., Sciaky, N., and Roth, B.L. (2015). Presto-Tango as an open-source resource for interrogation of the druggable human GPCRome. Nat. Struct. Mol. Biol. *22*, 362–369. https://doi.org/10.1038/nsmb.3014.

11. Jagadish, S., Barnea, G., Clandinin, T.R., and Axel, R. (2014). Identifying functional connections of the inner photoreceptors in Drosophila using Tango-Trace. Neuron *83*, 630–644. https://doi.org/10.1016/j.neuron.2014.06.025.

12. Liu, Y., Zeng, H., Pediani, J.D., Ward, R.J., Chen, L.Y., Wu, N., Ma, L., Tang, M., Yang, Y., An, S., et al. (2018). Visualization of the activation of the histamine H3 receptor (H3R) using novel fluorescence resonance energy transfer biosensors and their potential application to the study of H3R pharmacology. FEBS J. *285*, 2319–2336. https://doi.org/10.1111/febs.14484.

13. Schihada, H., Ma, X., Zabel, U., Vischer, H.F., Schulte, G., Leurs, R., Pockes, S., and Lohse, M.J. (2020). Development of a conformational histamine H(3) receptor biosensor for the synchronous screening of agonists and inverse agonists. ACS Sens. *5*, 1734–1742. https://doi.org/10.1021/acssensors.0c00397.

14. Erdogmus, S., Storch, U., Danner, L., Becker, J., Winter, M., Ziegler, N., Wirth, A., Offermanns, S., Hoffmann, C., Gudermann, T., and Mederos Y Schnitzler, M. (2019). Helix 8 is the essential structural motif of mechanosensitive GPCRs. Nat. Commun. *10*, 5784. https://doi.org/10.1038/s41467-019-13722-0.

15. Jing, M., Zhang, P., Wang, G., Feng, J., Mesik, L., Zeng, J., Jiang, H., Wang, S., Looby, J.C., Guagliardo, N.A., et al. (2018). A genetically encoded fluorescent acetylcholine indicator for in vitro and in vivo studies. Nat. Biotechnol. *36*, 726–737. https://doi.org/10.1038/nbt.4184.

16. Sun, F., Zeng, J., Jing, M., Zhou, J., Feng, J., Owen, S.F., Luo, Y., Li, F., Wang, H., Yamaguchi, T., et al. (2018). A genetically encoded fluorescent sensor enables rapid and specific detection of dopamine in flies, fish, and mice. Cell *174*. 481–496.e19. https://doi.org/10.1016/j.cell.2018.06.042.

17. Dong, A., He, K., Dudok, B., Farrell, J.S., Guan, W., Liput, D.J., Puhl, H.L., Cai, R., Wang, H., Duan, J., et al. (2022). A fluorescent sensor for spatiotemporally resolved imaging of endocannabinoid dynamics in vivo. Nat. Biotechnol. *40*, 787–798. https://doi.org/10.1038/s41587-021-01074-4.

18. Patriarchi, T., Cho, J.R., Merten, K., Howe, M.W., Marley, A., Xiong, W.H., Folk, R.W., Broussard, G.J., Liang, R., Jang, M.J., et al. (2018). Ultrafast neuronal imaging of dopamine dynamics with designed genetically encoded sensors. Science *360*, eaat4422. https://doi.org/10.1126/science.aat4422.

19. Wu, Z., Lin, D., and Li, Y. (2022). Pushing the frontiers: tools for monitoring neurotransmitters and neuromodulators. Nat. Rev. Neurosci. *23*, 257–274. https://doi.org/10.1038/s41583-022-00577-6.

20. Feng, J., Zhang, C., Lischinsky, J.E., Jing, M., Zhou, J., Wang, H., Zhang, Y., Dong, A., Wu, Z., Wu, H., et al. (2019). A genetically encoded fluorescent sensor for rapid and specific in vivo detection of norepinephrine. Neuron *102*. 745.e8–761.e8. https://doi.org/10.1016/j.neuron.2019.02.037.

21. Jing, M., Li, Y., Zeng, J., Huang, P., Skirzewski, M., Kljakic, O., Peng, W., Qian, T., Tan, K., Zou, J., et al. (2020). An optimized acetylcholine sensor for monitoring in vivo cholinergic activity. Nat. Methods *17*, 1139–1146. https://doi.org/10.1038/s41592-020-0953-2.

22. Sun, F., Zhou, J., Dai, B., Qian, T., Zeng, J., Li, X., Zhuo, Y., Zhang, Y., Wang, Y., Qian, C., et al. (2020). Next-generation GRAB sensors for monitoring dopaminergic activity in vivo. Nat. Methods *17*, 1156–1166. https://doi.org/10.1038/s41592-020-00981-9.

23. Wan, J., Peng, W., Li, X., Qian, T., Song, K., Zeng, J., Deng, F., Hao, S., Feng, J., Zhang, P., et al. (2021). A genetically encoded sensor for measuring serotonin dynamics. Nat. Neurosci. *24*, 746–752. https://doi.org/10.1038/s41593-021-00823-7.

24. Wu, Z., He, K., Chen, Y., Li, H., Pan, S., Li, B., Liu, T., Xi, F., Deng, F., Wang, H., et al. (2022). A sensitive GRAB sensor for detecting extracellular ATP in vitro and in vivo. Neuron *110*. 770–782.e5. https://doi.org/10.1016/j.neuron.2021.11.027.

25. Hirano, M., Ando, R., Shimozono, S., Sugiyama, M., Takeda, N., Kurokawa, H., Deguchi, R., Endo, K., Haga, K., Takai-Todaka, R., et al. (2022). A highly photostable and bright green fluorescent protein. Nat. Biotechnol. *40*, 1132–1142. https://doi.org/10.1038/s41587-022-01278-2.

26. Conklin, B.R., Farfel, Z., Lustig, K.D., Julius, D., and Bourne, H.R. (1993). Substitution of three amino acids switches receptor specificity of Gq alpha to that of Gi alpha. Nature *363*, 274–276. https://doi.org/10.1038/363274a0.

27. Inoue, A., Raimondi, F., Kadji, F.M.N., Singh, G., Kishi, T., Uwamizu, A., Ono, Y., Shinjo, Y., Ishida, S., Arang, N., et al. (2019). Illuminating G-protein-coupling selectivity of GPCRs. Cell *177*. 1933–1947.e25. https://doi.org/10.1016/j.cell.2019.04.044.

28. Scammell, T.E., Jackson, A.C., Franks, N.P., Wisden, W., and Dauvilliers, Y. (2019). Histamine: neural circuits and new medications. Sleep *42*, zsy183. https://doi.org/10.1093/sleep/zsy183.

29. Inagaki, N., Yamatodani, A., Ando-Yamamoto, M., Tohyama, M., Watanabe, T., and Wada, H. (1988). Organization of histaminergic fibers in the rat brain. J. Comp. Neurol. *273*, 283–300. https://doi.org/10.1002/cne.902730302.

30. Saper, C.B., Scammell, T.E., and Lu, J. (2005). Hypothalamic regulation of sleep and circadian rhythms. Nature *437*, 1257–1263. https://doi.org/10.1038/nature04284.

31. Strecker, R.E., Nalwalk, J., Dauphin, L.J., Thakkar, M.M., Chen, Y., Ramesh, V., Hough, L.B., and McCarley, R.W. (2002). Extracellular histamine levels in the feline preoptic/anterior hypothalamic area during natural sleep-wakefulness and prolonged wakefulness: an in vivo microdialysis study. Neuroscience *113*, 663–670. https://doi.org/10.1016/s0306-4522(02)00158-6.

32. Chu, M., Huang, Z.L., Qu, W.M., Eguchi, N., Yao, M.H., and Urade, Y. (2004). Extracellular histamine level in the frontal cortex is positively correlated with the amount of wakefulness in rats. Neurosci. Res. *49*, 417–420. https://doi.org/10.1016/j.neures.2004.05.001.

33. Parmentier, R., Anaclet, C., Guhennec, C., Brousseau, E., Bricout, D., Giboulot, T., Bozyczko-Coyne, D., Spiegel, K., Ohtsu, H., Williams, M., et al. (2007). The brain H3-receptor as a novel therapeutic target for vigilance and sleep-wake disorders. Biochem. Pharmacol. *73*, 1157–1171. https://doi.org/10.1016/j.bcp.2007.01.002.

34. Lohse, M.J., Hein, P., Hoffmann, C., Nikolaev, V.O., Vilardaga, J.P., and Bünemann, M. (2008). Kinetics of G-protein-coupled receptor signals in intact cells. Br. J. Pharmacol. *153* (*Suppl 1*), S125–S132. https://doi.org/10.1038/sj.bjp.0707656.

35. Ligneau, X., Lin, J., Vanni-Mercier, G., Jouvet, M., Muir, J.L., Ganellin, C.R., Stark, H., Elz, S., Schunack, W., and Schwartz, J. (1998). Neurochemical and behavioral effects of ciproxifan, a potent histamine H3-receptor antagonist. J. Pharmacol. Exp. Ther. *287*, 658–666.

36. Gondard, E., Anaclet, C., Akaoka, H., Guo, R.X., Zhang, M., Buda, C., Franco, P., Kotani, H., and Lin, J.S. (2013). Enhanced histaminergic neurotransmission and sleep-wake alterations, a study in histamine H3-receptor knock-out mice. Neuropsychopharmacology *38*, 1015–1031. https://doi.org/10.1038/npp.2012.266.

37. Ericson, H., Watanabe, T., and Köhler, C. (1987). Morphological analysis of the tuberomammillary nucleus in the rat brain: delineation of subgroups with antibody against L-histidine decarboxylase as a marker. J. Comp. Neurol. *263*, 1–24. https://doi.org/10.1002/cne.902630102.

Neuron
NeuroResource

 CellPress

38. Wada, H., Inagaki, N., Yamatodani, A., and Watanabe, T. (1991). Is the histaminergic neuron system a regulatory center for whole-brain activity? Trends Neurosci. *14*, 415–418.

39. Inagaki, N., Toda, K., Taniuchi, I., Panula, P., Yamatodani, A., Tohyama, M., Watanabe, T., and Wada, H. (1990). An analysis of histaminergic efferents of the tuberomammillary nucleus to the medial preoptic area and inferior colliculus of the rat. Exp. Brain Res. *80*, 374–380. https://doi.org/10.1007/BF00228164.

40. Zhou, F.M., Liang, Y., and Dani, J.A. (2001). Endogenous nicotinic cholinergic activity regulates dopamine release in the striatum. Nat. Neurosci. *4*, 1224–1229. https://doi.org/10.1038/nn769.

41. Liu, C., Cai, X., Ritzau-Jost, A., Kramer, P.F., Li, Y., Khaliq, Z.M., Hallermann, S., and Kaeser, P.S. (2022). An action potential initiation mechanism in distal axons for the control of dopamine release. Science *375*, 1378–1385. https://doi.org/10.1126/science.abn0532.

42. Panula, P., and Nuutinen, S. (2013). The histaminergic network in the brain: basic organization and role in disease. Nat. Rev. Neurosci. *14*, 472–487. https://doi.org/10.1038/nrn3526.

43. Ercan-Sencicek, A.G., Stillman, A.A., Ghosh, A.K., Bilguvar, K., O'Roak, B.J., Mason, C.E., Abbott, T., Gupta, A., King, R.A., Pauls, D.L., et al. (2010). L-histidine decarboxylase and Tourette's syndrome. N. Engl. J. Med. *362*, 1901–1908. https://doi.org/10.1056/NEJMoa0907006.

44. Hardie, R.C. (1987). Is histamine a neurotransmitter in insect photoreceptors? J. Comp. Physiol. A *161*, 201–213. https://doi.org/10.1007/BF00615241.

45. Hardie, R.C. (1989). A histamine-activated chloride channel involved in neurotransmission at a photoreceptor synapse. Nature *339*, 704–706. https://doi.org/10.1038/339704a0.

46. Ohtsu, H., Tanaka, S., Terui, T., Hori, Y., Makabe-Kobayashi, Y., Pejler, G., Tchougounova, E., Hellman, L., Gertsenstein, M., Hirasawa, N., et al. (2001). Mice lacking histidine decarboxylase exhibit abnormal mast cells. FEBS Lett. *502*, 53–56. https://doi.org/10.1016/s0014-5793(01)02663-1.

47. Yang, X.D., Ai, W., Asfaha, S., Bhagat, G., Friedman, R.A., Jin, G., Park, H., Shykind, B., Diacovo, T.G., Falus, A., and Wang, T.C. (2011). Histamine deficiency promotes inflammation-associated carcinogenesis through reduced myeloid maturation and accumulation of CD11b+Ly6G+ immature myeloid cells. Nat. Med. *17*, 87–95. https://doi.org/10.1038/nm.2278.

48. Barger, Z., Frye, C.G., Liu, D.Q., Dan, Y., and Bouchard, K.E. (2019). Robust, automated sleep scoring by a compact neural network with distributional shift correction. PLoS One *14*, e0224642. https://doi.org/10.1371/journal.pone.0224642.

🫆 CellPress

STAR★METHODS

KEY RESOURCES TABLE

REAGENT or RESOURCE	SOURCE	IDENTIFIER
Bacterial and virus strains		
AAV2/9-hSyn-HA1h (GRAB$_{HA1h}$)	Vigene Biosciences	N/A
AAV2/9-hSyn-HA1m (GRAB$_{HA1m}$)	Vigene Biosciences	N/A
AAV2/9-hSyn-HA1mut (GRAB$_{HA1mut}$)	Vigene Biosciences	N/A
AAV2/9-hSyn-mApple-CAAX	Vigene Biosciences	N/A
Chemicals, peptides, and recombinant proteins		
Histamine dihydrochloride (HA)	Tocris	Cat#3545
[3H]-histamine	PerkinElmer	Cat#NET732
Clemastine Fumarate	Cayman	Cat#14637
Ranitidine hydrochloride	Cayman	Cat#16939
Ciproxifan maleate	Cayman	Cat#29513
JNJ-7777120	Cayman	Cat#10011925
Histidine (His)	J&K Scientific (Beijing)	Cat#199604
Histaminol	Aladdin	Cat#H177821
Imidazoleacetic acid (ImAA)	Shanghai yuanye	Cat#S64493
Imidazolepyruvic acid (ImPA)	Sigma-Aldrich	Cat#78674
1-Methylhistamine (MHTM)	TargetMol	Cat#T8790
Methylimizoleacetic acid (MImAA)	Cayman	Cat#18815
Dopamine hydrochloride (DA)	Sigma-Aldrich	Cat#H8502
Norepinephrine bitartrate (NE)	Tocris	Cat#5169
Serotonin hydrochloride (5-HT)	Tocris	Cat#3547
Tyramine (TA)	Sigma-Aldrich	Cat#V900670
Octopamine hydrochloride (OA)	Tocris	Cat#2242
Adenosine (Ado)	Tocris	Cat#3624
L-Glutamic acid (Glu)	Sigma-Aldrich	Cat#V900408
Acetylcholine chloride (ACh)	Solar Biotech	Cat#G8320
γ-aminobutyric acid (GABA)	Tocris	Cat#0344
NanoLuc Luciferase Assay	Promega	Cat#N1110
Experimental models: Cell lines		
HEK293T	ATCC	Cat#CRL-3216; RRID: CVCL_0063
HEK293T cell line stably expressing HA1h	This paper	N/A
HTLA cells for Tango assay	Gift from Bryan L. Roth	N/A
Experimental models: Organisms/strains		
Rat: wild-type Sprague-Dawley rat pups (P0)	Beijing Vital River Laboratory Animal Technology Co., Ltd.	N/A
Mouse: wild-type C57BL/6	Beijing Vital River Laboratory Animal Technology Co., Ltd.	N/A
Mouse: wild-type BALB/c	Beijing Vital River Laboratory Animal Technology Co., Ltd.	N/A
Mouse: HDC KO (BALB/c background)	Gift from Xiangdong Yang[46,47]	N/A
Recombinant DNA		
pDisplay vector	Invitrogen	Cat#V66020
pDisplay-HA1h-IRES-mCherry-CAAX	This paper	N/A

(Continued on next page)

Neuron
NeuroResource

CellPress

Continued		
REAGENT or RESOURCE	SOURCE	IDENTIFIER
pDisplay-HA1m-IRES-mCherry-CAAX	This paper	N/A
pDisplay-HA1mut-IRES-mCherry-CAAX	This paper	N/A
pDisplay-HA1h-mScarlet	This paper	N/A
pDisplay-HA1m-mScarlet	This paper	N/A
hHRH4-SmBit	This paper	N/A
HA1h-SmBit	This paper	N/A
wbHRH1-SmBit	This paper	N/A
HA1m-SmBit	This paper	N/A
Software and algorithms		
AccuSleep	Barger et al.[48]	https://github.com/zekebarger/AccuSleep
Arduino	Arduino.cc	https://www.arduino.cc; RRID:SCR_017284
ImageJ	NIH	https://imagej.nih.gov/ij/; RRID: SCR_003070
Matlab R2020a	MathWorks	https://www.mathworks.com/; RRID:SCR_001622
Origin2020b	OriginLab	https://www.originlab.com/; RRID: SCR_014212
Spike2	Cambridge Electronic Design Ltd.	https://ced.co.uk/products/spkovin; RRID: SCR_000903
Code for 2-photon imaging analysis	This paper	https://doi.org/10.5281/zenodo.7638370

RESOURCE AVAILABILITY

Lead contact
Further information and requests for resources and reagents should be directed to and will be fulfilled by the lead contact, Yulong Li (yulongli@pku.edu.cn).

Materials availability
Plasmids expressing the sensors used in this study were deposited at Addgene (Addgene ID, HA1h, 190473. HA1m, 190474. HA1mut 190475. https://www.addgene.org/Yulong_Li/).

Data and code availability
- All imaging data reported in this paper will be shared by the lead contact upon request.
- The custom-written ImageJ macro code used in this study has been deposited at Zenodo and is publicly available as of the date of publication. DOIs are listed in the key resources table.
- Any additional information required to reanalyze the data reported in this paper is available from the lead contact upon request.

EXPERIMENTAL MODEL AND SUBJECT DETAILS

Animals
All experimental procedures involving animals were performed in accordance with the guidelines established by the Animal Care and Use Committee at Peking University. Wild-type C57BL/6j mice (8- to 12-weeks old) were obtained from the Beijing Vital River Laboratory and used to prepare the acute brain slices and for some *in vivo* mouse experiments. Histidine decarboxylase knockout (HDC KO) mice[46,47] (on a BALB/c background) were kindly provided by Dr. Xiangdong Yang at Fudan University; HDC KO and control littermates (8- to 12-weeks old) were used for *in vivo* recordings. Newborn wild-type Sprague-Dawley rat pups (P0) were obtained from the Beijing Vital River Laboratory and used to prepare primary cortical neuron cultures. Approximately equal numbers of male and female mice and rats were used. All animals were housed at 18–23°C in 40–60% humidity under a 12/12-h light/dark cycle, with food and water available *ad libitum*.

Recombinant AAV

The following AAV viruses were used to infect cultured cells and for in vivo expression (all packaged at Vigene Biosciences, China): AAV2/9-hSyn-HA1h (2.64×10^{13} GC/ml), AAV2/9-hSyn-HA1m (3.92×10^{13} GC/ml), AAV2/9-hSyn-HA1mut (9.03×10^{13} GC/ml), and AAV2/9-hSyn-mApple-CAAX (7.60×10^{13} GC/ml).

Cell lines

HEK293T cells were purchased from ATCC and verified based on their morphology observed by microscopy and an analysis of their growth curve; the cells were cultured at $37^\circ C$ in humidified air containing 5% CO_2 in DMEM (Biological Industries) supplemented with 10% (v/v) FBS (Gibco), penicillin (100 U/ml), and streptomycin (0.1 mg/ml) (Biological Industries). For expressing the GRAB$_{HA}$ sensors, HEK293T cells were plated on 96-well plates or 12-mm glass coverslips in 24-well plates and grown to 60-70% confluence, and then transfected using polyethylenimine (PEI) with 300 ng DNA per well (for 96-well plates) or 1 μg DNA per well (for 24-well plates) at a DNA:PEI ratio of 1:3. The culture medium was replaced with fresh medium 6-8 h after transfection, and fluorescence imaging was performed 24–48 h after transfection.

Primary cell cultures

Rat cortical neurons were prepared from P0 Sprague-Dawley rat pups. Approximately equal numbers of male and female rat pups were used. In brief, the cortex was dissected, and the neurons were dissociated in 0.25% trypsin–EDTA (Gibco), plated on 12-mm glass coverslips coated with poly-D-lysine (Sigma-Aldrich), and cultured in neurobasal medium (Gibco) containing 2% B-27 supplement (Gibco), 1% GlutaMAX (Gibco), and 1% penicillin-streptomycin (Gibco) at $37^\circ C$ in humidified air containing 5% CO_2. For viral infection, cultured neurons were infected with AAV2/9-hSyn-HA1h, AAV2/9-hSyn-HA1m, or AAV2/9-hSyn-HA1mut at 3–5 days in vitro (DIV3–DIV5), and fluorescence imaging was performed at DIV10–DIV14.

METHOD DETAILS

Molecular biology

The clones used in this study were generated using the Gibson assembly method. DNA fragments were amplified by PCR using primers (TSINGKE Biological Technology) with 25–30-bp overlap and then assembled using T5 exonuclease (New England Biolabs), Phusion DNA polymerase (Thermo Fisher Scientific), and Taq ligase (iCloning). All plasmid sequences were verified using Sanger sequencing (TSINGKE Biological Technology). To characterize the sensors in HEK293T cells, all cDNAs encoding the candidate GRAB$_{HA}$ sensors were cloned into the pDisplay vector with an upstream IgK leader sequence and a downstream IRES-mCherry-CAAX cassette to label the cell membrane and calibrate the sensor's fluorescence intensity. To characterize the sensors in cultured neurons, sequences encoding HA1h, HA1m, and HA1mut were cloned into the pAAV vector containing the human synapsin (hSyn) promoter. To measure downstream signaling using the Tango assay, genes encoding wild-type H$_1$R and H$_4$R, as well as the HA1h and HA1m sensors, were cloned into the pTango vector. To characterize the sensors' wavelength spectra, sequences encoding HA1h and HA1m were cloned into the pPacific vector containing a 3′ terminal repeat, IRES, puromycin gene, and a 5′ terminal repeat. Two mutations (S103P and S509G) were introduced into the pCS7-PiggyBAC vector (ViewSolid Biotech) to generate a hyperactive piggyBac transposase, which was used to generate stable cell lines expressing HA1h or HA1m.

Fluorescence imaging of cultured cells

Cultured cells were imaged using the Opera Phenix high-content screening system (PerkinElmer) and an inverted Ti-E A1 confocal microscope equipped with a 20x 0.4-numerical aperture (NA) objective, a 40x 0.6-NA objective, a 40x 1.15-NA water-immersion objective, a 488-nm laser, and a 561-nm laser. A 525/50 nm emission filter and a 600/30 nm emission filter were used to collect the GFP and RFP signals, respectively.

During fluorescence imaging, cells expressing the GRAB$_{HA}$ sensors were first bathed in Tyrode's solution and then imaged before and after addition of the indicated drugs at various concentrations. The change in fluorescence intensity of the GRAB$_{HA}$ sensors was calculated using the change in the GFP/RFP ratio and is expressed as $\Delta F/F_0$.

To measure the response kinetics of GRAB$_{HA}$ sensors in the rapid perfusion experiments using the line-scanning mode, the tip of a glass pipette containing 100 μM HA was placed near the sensor-expressing HEK293T cells. HA was puffed onto the cells from the pipette to measure the on-rate. To measure the off-rate, 1 mM of the appropriate antagonist (JNJ-7777120 to block HA1h, clemastine to block HA1m) was applied using a glass pipette to sensor-expressing cells bathed in HA (1 μM HA for cells expressing HA1h, 10 μM HA for cells expressing HA1m).

Screening of GRAB$_{HA}$ sensors
The development of HA1h

We selected human H$_4$R as the sensor scaffold, based on the good membrane trafficking property of H$_4$R chimera. The insertion site, the length, and the amino acid composition of the linker, as well as the critical residues in cpEGFP were optimized step by step based on the improvements of the sensor's maximum response and fluorescence.

Neuron
NeuroResource

CellPress

1. ICL3 replacement. We chose the ICL3-cpEGFP of previously developed $GRAB_{NE}$ to replace the corresponding ICL3 of hH_4R. 12 sites (K5.66 to N5.77) from N-term and 12 sites (G6.23 to L6.34) from C-term were chosen to generate the replacement library (Figure S2A). After screening the replacement sites, we generated a prototype HA sensor, namely HA0.1, with a 30% $\Delta F/F$ fluorescence response to 10 μM HA. The replacement sites of HA0.1 are between $Q211^{5.75}$ and $A302^{6.34}$ in hH_4R.

2. Linker length optimization. According to previous experience, the length and amino acid composition of the linker are critical for conformational coupling between the GPCR and the cpEGFP.[15–17,24] Therefore, we further optimized the length of linkers. The N-term linker of HA0.1 consists of 64 amino acids and the C-term linker has 11 amino acids. We truncated the linkers at both terminals simultaneously, truncating at every 5 amino acids and 2 amino acids of N-term and C-term respectively. We generated HA0.2 with 60% $\Delta F/F$ response to HA. For HA0.2, the N terminus linker has 18 amino acid residues and the C terminus linker has 9 residues left.

3. Linker sequence optimization. The amino acid composition of the linker is also critical to the sensor's dynamic range. We performed site-saturation mutagenesis on each residue of the linker and surrounding regions, followed by the combination of beneficial mutations. Specifically, point mutations were generated via PCR with primers containing NNB codon. We found the variant, namely HA0.5, with $Q211^{5.75}L$ and $G301^{6.33}A$ produced a ~220% increase in $\Delta F/F_0$.

4. cpEGFP optimization. Based on our experience on the development of GRAB sensors, we selected 12 residues in the cpEGFP (Figure S3C) for individual randomizations,[21,23] resulting in the HA1h sensor with a H18V mutation, which has ~400% response to 10 μM HA.

5. Mutant control. We engineered a mutant control, namely HA1mut, by introducing a $E211^{5.46}A$ mutation in HA1h.

The development of HA1m

We selected the wbH_1R-based scaffold for sensor optimization. Following the similar strategy with HA1h development, we optimized the insertion site and the amino acid composition of the linker region near the insertion site, as well as the critical residues in cpEGFP.

1. ICL3 replacement. After screening the insertion sites in the ICL3 of wbH_1R, we developed HA0.6m sensor with 220% fluorescent response to 100 μM HA. insertion site of HA0.6m is between $F261^{5.72}$ and $K513^{6.31}$ of wbH_1R.

2. Linker sequence optimization. We used site-saturation mutagenesis to create randomized point mutations at the linker and surrounding amino acids. We found variants with $K259^{5.70}A$ and $F261^{5.72}Q$ produced a ~530% increase in $\Delta F/F_0$.

3. cpEGFP optimization. We selected 9 residues in cpEGFP for randomization individually. We didn't find improved variants in this round of screening.

Spectra measurements

For 1P spectrum measurement, HEK293T cells expressing HA1h under the control of CAG promoter were plated in a 384-well plate in the absence or presence of 100 μM HA. Control cells used for background subtraction were transfected with an empty vector. Using a Safire2 multi-mode plate reader (Tecan), excitation spectra were measured from 300 to 520 nm at 5-nm increments and a bandwidth of 20 nm, while the emission spectrum was set to 560 nm with a 20-nm bandwidth. Emission spectra were measured from 500 to 700 nm at 5-nm increments and a bandwidth of 20 nm, while the excitation spectrum was set to 455 nm with a bandwidth of 20 nm. For the HA1m sensor, the plasmid expressing HA1m or an empty vector was transfected into HEK293T cells in 6-well plates; 24–36 h after transfection, the cells were harvested using trypsin, washed with PBS, resuspended in Tyrode's solution in the absence or presence of 100 μM HA, and plated into a 384-well plate, followed by the spectra measurements described above. For 2P spectrum measurement, plasmids expressing HA1m or HA1h were transfected into HEK293T cells on 12-mm coverslips, after 18 h, the cells in Tyrode's solution in the absence or presence of 100 μM HA were imaged by an Ultima Investigator 2P microscope (Bruker) equipped with a ×20, 1.00-NA objective (Olympus) and an InSight X3 tunable laser (Spectra-Physics). Images were captured when cells were excited from 680 to 1050 nm with a step size of 10 nm.

Photobleaching measurement

Plasmids for expression of HA1h and HA1m as well as EGFP-CAAX or StayGold-CAAX were transfected into HEK293T cells on 12-mm coverslips (for confocal) or in 96 plates (for Operetta CLS) respectively. For imaging after 24h transfection, the culture medium was replaced with Tyrode's solution, and 100 μM HA was applied in Tyrode's solution. Using the confocal microscopy, photobleaching was measured with a ×40 oil objective lens (UPlanSApo ×40/1.30 NA) and the 488-nm laser at a power of 100 μW. While, using the Operetta CLS wide field fluorescence imaging system, photobleaching was measured with a ×20 water objective lens (UPlanSApo ×20/1.0 NA) with the 488-nm illumination at a LED power of 2.5 mW and the illumination intensity was 5.1 mW/cm^2.

G_{qi} calcium imaging assay

Plasmids expressing the $GRAB_{HA}$ sensors, H_1R-EGFP, or H_4R-EGFP were co-transfected with a construct expressing jRGECO1a-P2A-G_{q-i1} into HEK293T cells plated on 12-mm coverslips; 24–48 h after transfection, the cells were imaged using a Ti-E A1 confocal microscope (Nikon) as described above. The indicated concentrations of HA were then applied by bath application and removed using a custom-made perfusion system.

Tango assay

Plasmids expressing wild-type H_1R, wild-type H_4R, HA1h, or HA1m were transfected into HTLA cells in 6-well plates; 24 h after transfection, the cells were harvested using trypsin and plated in 96-well plates. HA was then applied at a final concentration ranging from 1 nM to 1 mM, and the cells were cultured for an additional 12 h to allow for luciferase expression. Bright-Glo (Luciferase Assay System, Promega) was then added to a final concentration of 5 μM, and luminescence was measured using a VICTOR X5 multilabel plate reader (PerkinElmer).

[³H]histamine competition binding assay

Plasmids expressing wild-type H_4R or HA1h were transfected into HEK293T cells in 10 cm dishes; 48 h after transfection, the cells were collected, centrifuged at 2000g for 10 min at 4°C, resuspended in 50 mM Tris-HCl binding buffer (pH7.4), and sonicated for 10 sec using a Branson sonifier 250 (Boom bv., Meppel, The Netherlands). The cell homogenates were incubated with $\sim$8.5 nM [³H]-histamine in the absence of presence of 30 μM unlabeled compounds in a total volume of 100 μl/well at 25°C on a shaker (600 rpm). After 2 h, the incubations were terminated by rapid filtration through 0.5% (v/v) polyethylenimine pre-soaked GF/C filter-plates using a 96-well Filtermate harvester (PerkinElmer), followed by four rapid washes with ice-cold binding buffer. The GF/C filter-plates were dried at 52°C and 25 μl Microscint-O was added to each well to quantify radioactivity using a Microbeta Wallac Trilux scintillation counter (PerkinElmer). Saturation binding of [³H]histamine was measured with increasing concentrations of [³H]histamine in the absence or presence of 50 microM JNJ7777120 to detect total and nonspecific binding respectively. The binding affinity (K_d) values were determined using nonlinear fitting (One site – total and nonspecific binding) in GraphPad Prism 9.4.0.

Two-photon fluorescence imaging of mouse acute brain slices

For AAV injection, adult wild-type C57BL/6N mice were firstly anesthetized by an i.p. injection of Avertin (500 mg/kg, Sigma-Aldrich), and then fixed in a stereotaxic frame (RWD Life Science) for injection of the AAV expressing hSyn-HA1m (300 nl per site) using a micro-syringe pump (Nanoliter 2000 Injector, World Precision Instruments). The AAV was injected into the PFC of the left hemisphere of C57BL/6N mice using the following coordinates: AP: +1.9 mm relative to Bregma, ML: -0.3 mm, and DV: -1.8 mm below the dura.

For slice preparation, 2-3 weeks after virus injection, mice were deeply anesthetized again with an i.p. injection of Avertin, and then transcardial perfusion was rapidly performed using cold oxygenated slicing buffer containing (in mM): 110 Choline-Cl, 25 $NaHCO_3$, 25 Glucose, 7 $MgCl_2$, 2.5 KCl, 1.3 Na ascorbate, 1 NaH_2PO_4, 0.5 $CaCl_2$, and 0.6 Na pyruvate. The isolated brains were subsequently immersed into the oxygenated slicing buffer, and the cerebellum was trimmed using a razor blade. The caudal sides were then glued on the cutting stage of a VT1200 vibratome (Leica) and sectioned into 300-μm thick coronal slices. Brain slices containing the PFC region were incubated at 34°C for $\sim$40 min in the oxygen-saturated Ringer's buffer containing (in mM): 125 NaCl, 25 $NaHCO_3$, 25 Glucose, 2.5 KCl, 2 $CaCl_2$, 1.3 $MgCl_2$, 1.3 Na ascorbate, 1 NaH_2PO_4, and 0.6 Na pyruvate.

For two-photon imaging, the HA1m-expressing slices were transferred into a perfusion chamber in an Ultima Investigator 2P microscope (Bruker) equipped with a 20× /1.00-NA water-immersion objective and an InSight X3 laser (Spectra-Physics). The laser wavelength was tuned to 920 nm for measuring the fluorescence of HA1m using a 495-540 nm filter. A homemade bipolar electrode (cat. #WE30031.0A3, MicroProbes) was placed onto the slice surface near the PFC under fluorescence guidance. Fluorescence was then recorded at video frame rates of 0.3259 s/frame, with a resolution of 256×256 pixels. The stimulation voltage was set at 4-6 V with the duration of each stimulation at 1 ms. Stimulation and imaging were synchronized through a custom-written program running on an Arduino board.

Surgery for virus injection, placement of EEG and EMG electrodes, and fiber implantation

Adult mice were anesthetized with 1.5% isoflurane, and 2% lidocaine hydrochloride was injected subcutaneously under the scalp; the mouse was then placed on a stereotaxic frame (RWD Life Science). The skull was exposed, and small craniotomy holes were prepared for virus injection, into which a total of approximately 300 nl AAV9-hSyn-HA1h, AAV9-hSyn-HA1m, or AAV9-hSyn-HA1mut virus was microinjected into the PFC (AP: +1.9 mm relative to Bregma, ML: -0.3 mm, DV: 1.9 mm below the dura) and/or POA (AP: 0 mm relative to Bregma, ML: -0.6 mm, DV: 4.9 mm below the dura) via a fine glass pipette and micro-syringe pump (Nanoliter 2010 injector, World Precision Instruments).

For recording the fluorescence signals, a 200-μm optical fiber cannula (Fiber core: 200 μm; numerical aperture: 0.37; Inper, Zhejiang, China) was implanted 0.1 mm above the virus injection sites.

To record the animal's sleep-wake state, EEG electrodes were implanted into the craniotomy holes over the frontal cortex and visual cortex, and EMG wires were placed bilaterally into the trapezius muscles. The electrodes were attached to a microconnector and fixed to the skull using dental cement.

Fiber photometry recording and analysis

A fiber photometry system (Thinker Tech, Nanjing, China) was used to record the fluorescence signals in freely moving mice. Blue (473-nm) LED light (Cree LED) was bandpass filtered (470/10 nm, model 65-144, Edmund Optics), reflected by a dichroic mirror (model 67-079, Edmund Optics), and then focused using a 20x objective lens (Olympus). An optical fiber guided the light between the commutator and the implanted optical fiber cannula. The excitation light power at the tip of the optical fiber was adjusted 20-30 μW and delivered at 100 Hz with 5 ms pulse duration when the recording lasted <24 h; the light power was adjusted to a lower

Neuron
NeuroResource

 CellPress

level (10-20 µW) and was delivered at 10 Hz when the recording lasted >24 h in order to minimize photobleaching. The green fluorescence was bandpass filtered (525/15 nm, model 86-354, Edmund Optics) and collected using a photomultiplier tube (model H10721-210, Hamamatsu). An amplifier (model C7319, Hamamatsu) was used to convert the current output from the photomultiplier tube to a voltage signal and was passed through a low-pass filter. The analog voltage signals were then digitized using an acquisition card (National Instruments). To minimize autofluorescence of the optical fiber, the recording fiber was photobleached using a high-power LED before recording. Background autofluorescence was subtracted from the recorded signals in the subsequent analysis.

The photometry data were analyzed using a custom program written in MATLAB. To calculate $\Delta F/F_0$, baseline values were measured during REM sleep with no apparent fluctuations. To compare the change in fluorescence between animals, the z-score–transformed $\Delta F/F_0$ was further normalized using the standard deviation of the baseline signals.

Polysomnographic recording and analysis

We used the EEG and EMG recordings to determine the animal's sleep-wake state. The EEG and EMG electrode microconnectors were connected via a flexible cable and attached to an electric slip ring to allow the mice to move freely. The cortical EEG and neck EMG signals were amplified (NL104A, Digitimer), filtered (NL125/6, Digitimer), digitized using a Power1401 digitizer (Cambridge Electronic Design Ltd.), and recorded using Spike2 software (Cambridge Electronic Design Ltd.) at a sampling rate of 1000 Hz. The polysomnographic signals were filtered (EEG: 0.5-100 Hz, EMG: 30-500 Hz) and semi-automatically scored off-line in 4-s epochs of wakefulness, REM sleep, and NREM sleep using AccuSleep (https://github.com/zekebarger/AccuSleep)[48]; the defined sleep-wake stages were examined visually and corrected if necessary. Wakefulness was defined as desynchronized low-amplitude EEG activity and high-amplitude EMG activity with phasic bursts. NREM sleep was defined as synchronized EEG with high-amplitude delta rhythm (0.5-4 Hz) and low EMG activity. REM sleep was defined as a pronounced theta rhythm (6-10 Hz) and low EMG activity. EEG spectral analysis was estimated using a short-time fast Fourier transform (FFT).

QUANTIFICATION AND STATISTICAL ANALYSIS

The animals and cells in the experiments were randomly assigned to different groups at sample sizes that were determined based on previous studies.[22] Imaging data from cultured HEK293T cells, cultured rat cortical neurons, and acute mouse brain slices were processed using ImageJ software (NIH) and analyzed using custom MATLAB code. Exponential-function fitting was used to correct for slight photobleaching. Background levels measured outside the region of interest in the pseudocolor images were subtracted using ImageJ. The corrected fluorescence was used to calculate the change in fluorescence ($\Delta F/F_0$) using the formula $(F - F_0)/F_0$, where F_0 is the baseline fluorescence signal before stimulation or drugs application.

Origin 2020 (OriginLab) and Prism 8 & 9 (GraphPad) were used to perform the statistical analyses. Except where indicated otherwise, all summary data are presented as the mean ± sem. The paired or unpaired Student's *t*-test was used to compare two groups, and a one-way analysis of variance (ANOVA) was used to compare more than two groups. All statistical tests were two-tailed, and differences were considered statistically significant at $P < 0.05$.